Preprints of the 21st IFAC World Congress (Virtual)
Berlin, Germany, July 12-17, 2020

Adaptive Robust Generalized Dynamic Inversion Quadrotor Control

Uzair Ansari * **Abdulrahman H. Bajodah** **

* *Research Scholar, Center of Excellence in Intelligent Engineering Systems, King Abdulaziz University, Jeddah 21589, Saudi Arabia, (e-mail: uansari@stu.kau.edu.sa).*
** *Professor, Department of Aerospace Engineering, King Abdulaziz University, Jeddah 21589, Saudi Arabia, (e-mail: abajodah@kau.edu.sa)*

Abstract: This paper proposes a two loops control system structure for position and attitude of the Quadrotor flying vehicle. To control the Quadrotor's center of gravity position in the instantaneous horizontal inertial planes, a small disturbance linearization-based Proportional-Derivative controller is employed in the outer (position) loop to provide reference pitch and roll tilting commands to the inner (attitude) loop. The outer loop also generates the thrust command required to track desired altitude trajectories. The inner loop utilizes a novel Adaptive Robust Generalized Dynamic Inversion (ARGDI) control design that is made by augmenting a direct adaptive control element in the baseline Robust Generalized Dynamic Inversion control system. The adaptive control law is obtained via a control Lyapunov function, and it aims to reduce the dependency of the control system on the geometric and inertia parameters of the Quadrotor in order to overcome control performance degradation due to modeling and parametric uncertainties, and due to external wind disturbances and dynamic scaling of the Moore-Penrose Generalized inverse. Computer simulations are performed in the Matlab/Simulink environment on a six DOFs Quadrotor model to demonstrate the robust globally asymptotically stable performance of the two loops control system. Additionally, performance of the inner ARGDI attitude control loop is tested on an experimental Quanser's three DOFs Hover test bench.

Keywords: Adaptive Robust Generalized Dynamic Inversion, Sliding Mode Control, Small disturbance theory, Quadrotor control, Global asymptotic stability.

1. INTRODUCTION

Designing an effective Quadrotor flight control system is a challenging task due to its nonlinear complex dynamics and because of stability and performance concerns regarding modeling and parametric uncertainties, external disturbances, and actuator dissimilarities, see, e.g., Mahony et al. (2012). To address these problems, numerous linear and nonlinear control methodologies were investigated in the Quadrotor control literature.

Among the linear control methodologies, PID and LQR control designs were implemented on Quadrotor platforms, e.g., Bouabdallah et al. (2004). However, linear control methodologies have limited capabilities in achieving good performance over wide ranges of operations and strong nonlinearities. To perform high performance maneuvers with good tracking performance, several nonlinear control methodologies have been developed for the Quadrotor vehicles. Among the nonlinear Quadrotor control designs that appear in literature are adaptive control Zhou et al. (2018), Sliding Mode Control (SMC) L'afflitto et al. (2018), Model Predictive Control (MPC) Falanga et al. (2018), Integral Back-Stepping Control Poultney et al. (2019), Fuzzy Logic Control Vitzilaios and Tsourveloudis (2009), Nonlinear Dynamic Inversion (NDI) Das (2018), etc.

The NDI control design is attractive because of its simplicity, intuitiveness, and practicality. However, among the limitations of the NDI control approach is the requirement of exact mathematical modeling of the controlled plant's system dynamics, performance degradation because of the simplifying approximations that are needed to invert the plant dynamics, elimination of useful nonlinearities, the square dimensionality restriction, and the possibilities of square inversion singular configurations.

On the other hand, the Generalized Dynamic Inversion (GDI) control methodology has been capable of overcoming the shortcomings and challenges of NDI Ansari et al. (2018). The methodology is based on prescribing one or more virtual differential state constraints that express the prime control design objectives. The differential state constraints are evaluated along the trajectories of the dynamical system, and are imposed on its closed loop dynamics by means of the dynamically scaled Moore-Penrose Generalized Inverse (MPGI). If the number of virtual constraints is less than the number of control variables then another component of the control vector that is orthogonal to the range space of the MPGI provides an extra design

freedom that can be utilized to satisfy other control design objectives. The GDI control methodology has been applied to numerous aerospace and robotics applications, see, e.g., Ansari et al. (2019a); Ansari and Bajodah (2017b,a).

This paper presents a two loops direct adaptive control design structure that is based on the GDI control design methodology. A Proportional Derivative (PD) constrained control type is applied in the outer (position) loop on Quadrotor's dynamical equations of motion that are linearized via the small disturbance theory to produce pitch and roll attitude commands while controlling the quadrotor's altitude. The inner (attitude) GDI control loop produces the control torque commands for desired roll, pitch, and yaw attitude tracking. To enhance the GDI control loop robustness against system uncertainties and external disturbances and MPGI dynamic scaling, a SMC element is augmented with the baseline controller resulting in the Robust GDI (RGDI) control law. Finally, an adaptive control loop is augmented within the inner loop to further reduce the dependency of the Robust GDI (RGDI) control design on the inertia parameters of the Quadrotor. The adaptive RGDI (ARGDI) control system performance is validated through numerical simulations on a six Degrees of Freedom (DOFs) simulator of X4-flyer quadrotor considering nominal and perturbed flight conditions.

A dynamic modeling brief of the Quadrotor is presented in section 2. The two loops control system is described in section 3. The outer position and inner attitude control systems are designed in sections 4 and 5, respectively. The computer simulations and the experimental results are given in section 6, and the paper is concluded in section 7.

2. QUADROTOR MODELING

The Quadrotor's main frame is assumed to be a rigid body, and its center of gravity (CG) is assumed to coincide with the origin $O_{\mathbf{B}}$ of the body coordinate system. The Quadrotor's body-fixed reference frame is denoted by $\mathbf{B}(x_b, y_b, z_b)$, and the inertial Earth-fixed reference frame is denoted by $\mathbf{E}(x_e, y_e, z_e)$. The total Quadrotor's thrust force in the negative z_b direction is given by

$$T = \sum_{i=1}^{4} T_i = b \sum_{i=1}^{4} \omega_i^2, \quad i = 1, 2, 3, 4 \tag{1}$$

where T_i is the thrust force of the i^{th} rotor in the negative z_b direction, b is the lift coefficient of an individual rotor and is assumed to be identical for the four rotors, and ω_i is angular speed of the i^{th} rotor, and it is negative for $i = 1, 3$ and positive for $i = 2, 4$. The torques generated by the rotors about the x_b axis (τ_x rolling torque), y_b axis (τ_y pitching torque), and z_b axis (τ_z yawing torque) are given by

$$\tau_x = db(\omega_4^2 - \omega_2^2) \tag{2}$$

$$\tau_y = db(\omega_3^2 - \omega_1^2) \tag{3}$$

$$\tau_z = k(\omega_1^2 - \omega_2^2 + \omega_3^2 - \omega_4^2) \tag{4}$$

where d is the moment arm of T_i about $O_{\mathbf{B}}$, $i = 1, \cdots, 4$. The yawing moment τ_z that is given by (4) is generated by the rotors' drag forces that tend to rotate the Quadrotor in opposite directions by creating reaction torques on the Quadrotor's body, where the drag-to-moment coefficient k is determined experimentally Leishman (2002); Mahony et al. (2012). The Quadrotor is an under-actuated dynamical system having a 4-dimensional input vector

$$\mathbf{u} = [T \ \tau_x \ \tau_y \ \tau_z]^T \tag{5}$$

and a twelve dimensional controlled state vector

$$\mathbf{x} = \begin{bmatrix} x_e & y_e & z_e & \dot{x}_e & \dot{y}_e & \dot{z}_e & \phi & \theta & \psi & \dot{\phi} & \dot{\theta} & \dot{\psi} \end{bmatrix}^T \tag{6}$$

where ϕ, θ, and ψ are respectively Euler's roll, pitch, and yaw angles that are used as coordinates of angular orientation Nelson (1997). The relation between the input vector $\mathbf{u}$ and the angular speeds of the rotors is given by Mahony et al. (2012)

$$\mathbf{u} = \mathbf{R} \begin{bmatrix} \omega_1^2 & \omega_2^2 & \omega_3^2 & \omega_4^2 \end{bmatrix}^T \tag{7}$$

where $\mathbf{R}$ is the 4×4 full rank constant matrix given by

$$\mathbf{R} = \begin{bmatrix} -b & -b & -b & -b \\ 0 & -db & 0 & db \\ db & 0 & -db & 0 \\ k & -k & k & -k \end{bmatrix}. \tag{8}$$

The translational Quadrotor's kinematics in $\mathbf{E}$ is given by the vector equation

$$\dot{\boldsymbol{\mu}} = \mathbf{v} = [\dot{x}_e \ \dot{y}_e \ \dot{z}_e]^T \tag{9}$$

where $\boldsymbol{\mu}$ and $\mathbf{v}$ are the inertial displacement and velocity vectors of the Quadrotor's center of gravity $O_{\mathbf{B}}$, respectively. The translational Quadrotor's dynamics are modeled by Newton's equations of motion

$$m \frac{^{\mathbf{E}}d\mathbf{v}}{dt} = mg\mathbf{n_E} - T\mathbf{n_B} \tag{10}$$

where m is the Quadrotor's mass, g is the acceleration due to gravity, and

$$\frac{^{\mathbf{E}}d\mathbf{v}}{dt} = \dot{\mathbf{v}} = [\ddot{x}_e \ \ddot{y}_e \ \ddot{z}_e]^T \tag{11}$$

is the time derivative of $\mathbf{v}$ relative to $\mathbf{E}$, and the unit vectors $\mathbf{n_E}$ and $\mathbf{n_B}$ are in the positive z_e and z_b directions, respectively. Expressing (10) in $\mathbf{E}$ and solving for the inertial accelerations $\ddot{x}_e$, $\ddot{y}_e$, and $\ddot{z}_e$ yield

$$\begin{bmatrix} \ddot{x}_e \\ \ddot{y}_e \\ \ddot{z}_e \end{bmatrix} = \begin{bmatrix} 0 \\ 0 \\ g \end{bmatrix} - \mathbf{L_{EB}} \begin{bmatrix} 0 \\ 0 \\ \dfrac{T}{m} \end{bmatrix} \tag{12}$$

where $\mathbf{L_{EB}}$ is the $L_x(-\phi) \rightarrow L_y(-\theta) \rightarrow L_z(-\psi)$ transformation matrix from $\mathbf{B}$ to $\mathbf{E}$, see, e.g., Nelson (1997). The final form of (12) is

$$\begin{bmatrix} \ddot{x}_e \\ \ddot{y}_e \\ \ddot{z}_e \end{bmatrix} = \begin{bmatrix} 0 \\ 0 \\ g \end{bmatrix} - \begin{bmatrix} s_\psi s_\phi + c_\psi s_\theta c_\phi \\ -c_\psi s_\phi + s_\psi s_\theta c_\phi \\ c_\theta c_\phi \end{bmatrix} \frac{T}{m} \tag{13}$$

where the abbreviations c_ψ and s_θ refer to $\cos\psi$ and $\sin\theta$, etc. Denote the angular velocity vector of $\mathbf{B}$ with respect to $\mathbf{E}$ by $\boldsymbol{\Omega}$, and express it in $\mathbf{B}$ as

$$\boldsymbol{\Omega} = [p \ q \ r]^T \tag{14}$$

and denote the angular velocity vector of the i^{th} rotor with respect to $\mathbf{E}$ by $\boldsymbol{\Omega}_{\mathbf{r_i}}$, and express it in $\mathbf{B}$ as

$$\boldsymbol{\Omega}_{\mathbf{r_i}} = [p \ q \ r + \omega_i]^T. \tag{15}$$

The Quadrotor's rotational kinematics is given by the relation between the time rates of Euler's angles and the body components of $\boldsymbol{\Omega}$ as Nelson (1997)

$$\begin{bmatrix}\dot{\phi}\\ \dot{\theta}\\ \dot{\psi}\end{bmatrix} = \begin{bmatrix}1 & s_\phi t_\theta & c_\phi t_\theta\\ 0 & c_\phi & -s_\phi\\ 0 & s_\phi/c_\theta & c_\phi/c_\theta\end{bmatrix}\begin{bmatrix}p\\ q\\ r\end{bmatrix} \tag{16}$$

where t_θ stands for $\tan\theta$. Equation (16) is rewritten compactly as

$$\dot{\mathbf{\Psi}} = \mathbf{\Gamma}(\phi,\theta)\mathbf{\Omega}. \tag{17}$$

The angular momentum vector of the Quadrotor about $O_{\mathbf{B}}$ is

$$\mathbf{H} = \mathbf{J}\mathbf{\Omega} + \mathbf{J_r}\sum_{i=1}^{4}\mathbf{\Omega_{r_i}} \tag{18}$$

where $\mathbf{J} = diag\,[J_x,\ J_y,\ J_z]$ is the 3×3 Quadrotor's main frame's diagonal inertia matrix, such that J_x, J_y, and J_z are the principal moments of inertia constants, and $\mathbf{J_r} = diag\,[0,\ 0,\ J_r]$ is the approximate 3×3 rotor's diagonal inertia matrix, where J_r is the rotor's polar moment of inertia constant about the rotor's axis of rotation, and is assumed identical for the four rotors, and the rotor's transverse moments of inertia constants about the axes in the plane of rotor's rotation are assumed ignorably small. The time derivative of $\mathbf{H}$ relative to $\mathbf{E}$ is given by the basic (transport) kinematical equation Kasdin and Paley (2011) as

$$\frac{^{\mathbf{E}}d\mathbf{H}}{dt} = \frac{^{\mathbf{B}}d\mathbf{H}}{dt} + \mathbf{\Omega}\times\mathbf{H} = \mathbf{J}\dot{\mathbf{\Omega}} + \mathbf{\Omega}^{\times}\mathbf{J}\mathbf{\Omega} + \mathbf{J_r}\sum_{i=1}^{4}\dot{\mathbf{\Omega}}_{\mathbf{r_i}} + \mathbf{\Omega}^{\times}\mathbf{J_r}\sum_{i=1}^{4}\mathbf{\Omega_{r_i}} \tag{19}$$

where $\dot{\mathbf{\Omega}} = [\dot{p}\ \dot{q}\ \dot{r}]^T$ and $\dot{\mathbf{\Omega}}_{\mathbf{r_i}} = [\dot{p}\ \dot{q}\ \dot{r}+\dot{\omega}_i]^T$ are respectively the time derivatives of $\mathbf{\Omega}$ and $\mathbf{\Omega_{r_i}}$ relative to $\mathbf{B}$, and $\mathbf{\Omega}^{\times}$ is the cross product matrix that corresponds to $\mathbf{\Omega}$, and is given by

$$\mathbf{\Omega}^{\times} = \begin{bmatrix}0 & -r & q\\ r & 0 & -p\\ -q & p & 0\end{bmatrix}. \tag{20}$$

The rotational Quadrotor's dynamics are modeled by Euler's equations of motion

$$\frac{^{\mathbf{E}}d\mathbf{H}}{dt} = \boldsymbol{\tau} \tag{21}$$

where $\boldsymbol{\tau} = [\tau_x\ \tau_y\ \tau_z]^T$. Substituting (19) in (21) and solving for $\dot{\mathbf{\Omega}}$ yields the following Quadrotor's rotational dynamical equations of motion in $\mathbf{B}$

$$\dot{\mathbf{\Omega}} = -\mathbf{J}^{-1}\Big(\mathbf{\Omega}^{\times}\mathbf{J}\mathbf{\Omega} + \mathbf{J_r}\sum_{i=1}^{4}\dot{\mathbf{\Omega}}_{\mathbf{r_i}} + \mathbf{\Omega}^{\times}\mathbf{J_r}\sum_{i=1}^{4}\mathbf{\Omega_{r_i}} - \boldsymbol{\tau}\Big). \tag{22}$$

The acceleration form of Euler's kinematical equations (17) is derived next to have the control input appear in the equations. The time derivative of $\dot{\mathbf{\Psi}}$ is

$$\ddot{\mathbf{\Psi}} = \dot{\mathbf{\Gamma}}(\phi,\theta,\dot{\phi},\dot{\theta})\mathbf{\Omega} + \mathbf{\Gamma}(\phi,\theta)\dot{\mathbf{\Omega}} \tag{23}$$

where $\dot{\mathbf{\Gamma}}(\phi,\theta,\dot{\phi},\dot{\theta})$ is the element-wise time derivative of $\mathbf{\Gamma}(\phi,\theta)$. Substituting (22) in (23) yields the following compact expression for $\ddot{\mathbf{\Psi}}$

$$\ddot{\mathbf{\Psi}} = \mathbf{F} + \mathbf{G}\boldsymbol{\tau} \tag{24}$$

where

$$\mathbf{F} = \dot{\mathbf{\Gamma}}(\phi,\theta,\dot{\phi},\dot{\theta})\mathbf{\Omega} - \mathbf{\Gamma}(\phi,\theta)\mathbf{J}^{-1}\Big(\mathbf{\Omega}^{\times}\mathbf{J}\mathbf{\Omega} + \mathbf{J_r}\sum_{i=1}^{4}\dot{\mathbf{\Omega}}_{\mathbf{r_i}} + \mathbf{\Omega}^{\times}\mathbf{J_r}\sum_{i=1}^{4}\mathbf{\Omega_{r_i}}\Big) \tag{25}$$

and

$$\mathbf{G} = \mathbf{\Gamma}\mathbf{J}^{-1}. \tag{26}$$

Moreover, because $|r| << |\omega_i|$ and $|\dot{r}| << |\dot{\omega}_i|$, (22) is approximated by omitting r and $\dot{r}$ in the expressions of $\mathbf{\Omega_{r_i}}$ and $\dot{\mathbf{\Omega}}_{\mathbf{r_i}}$.

3. ARGDI CONTROL SYSTEM STRUCTURE

In proposed two loops structured control system, the outer (slow) positional loop utilizes PD control to generate reference pitch and roll tilting commands to inner attitude loop. Additionally, the outer loop controls the altitude of the quadrotor by producing the thrust control variable. The inner (fast) attitude control loop utilizes the proposed ARGDI design to control the yaw, pitch and roll attitude variables by producing the three control torque variables.

4. PD CONTROL FOR OUTER LOOP

The desired acceleration commands along x_e and y_e directions are computed by replacing $\ddot{x}_e$ and $\ddot{y}_e$ by $\ddot{x}_{ed}$ and $\ddot{y}_{ed}$, and ϕ and θ by ϕ_r and θ_r respectively in (12), resulting in

$$\begin{bmatrix}\ddot{x}_{ed}\\ \ddot{y}_{ed}\end{bmatrix} = -\begin{bmatrix}s_\psi s_{(\phi+\triangle\phi)} + c_\psi s_{(\theta+\triangle\theta)} c_{(\phi+\triangle\phi)}\\ -c_\psi s_{(\phi+\triangle\phi)} + s_\psi s_{(\theta+\triangle\theta)} c_{(\phi+\triangle\phi)}\end{bmatrix}\frac{T}{m} \tag{27}$$

where

$$\phi_r(t) = \phi(t) + \triangle\phi(t) \tag{28}$$

$$\theta_r(t) = \theta(t) + \triangle\theta(t) \tag{29}$$

The variables $\triangle\theta$ and $\triangle\phi$ representing the reference tilting commands generated by the outer positional loop to stabilize the positional coordinates. The trigonometric functions about the instantaneous values $\phi(t)$ and $\theta(t)$ are expanded using small disturbance theory assumptions yields the following linear system

$$\begin{bmatrix}\ddot{x}_{ed}\\ \ddot{y}_{ed}\end{bmatrix} = \mathbf{M}\mathbf{u} + \mathbf{N} \tag{30}$$

where

$$\mathbf{M} = -\frac{T}{m}\begin{bmatrix}s_\psi c_\phi - c_\psi s_\theta s_\phi & c_\psi c_\theta c_\phi\\ -c_\psi c_\phi - s_\psi s_\theta s_\phi & s_\psi c_\theta c_\phi\end{bmatrix}$$

$$\mathbf{N} = -\frac{T}{m}\begin{bmatrix}s_\psi s_\phi + c_\psi s_\theta c_\phi\\ -c_\psi s_\phi + s_\psi s_\theta c_\phi\end{bmatrix}, \qquad \mathbf{u} = \begin{bmatrix}\triangle\phi\\ \triangle\theta\end{bmatrix}.$$

The control expression is obtained by solving (30) as

$$\mathbf{u} = \mathbf{M}^{-1}\left(\begin{bmatrix}\ddot{x}_{ed}\\ \ddot{y}_{ed}\end{bmatrix} - \mathbf{N}\right). \tag{31}$$

The virtual dynamics of the Quadrotor's center of gravity O_B in arbitrary horizontal inertial planes is chosen to be in the following form

$$\ddot{x}_e + c_1(\dot{x}_e - \dot{x}_{ed}) + c_2(x_e - x_{ed}) = \ddot{x}_{ed} \tag{32}$$

and

$$\ddot{y}_e + c_3(\dot{y}_e - \dot{y}_{ed}) + c_4(y_e - y_{ed}) = \ddot{y}_{ed} \tag{33}$$

where c_1, c_2, c_3, and c_4 are strictly positive scalars. The control expression $\mathbf{u}$ is obtained by substituting $\ddot{x}_{ed}$ and $\ddot{y}_{ed}$ from (32) and (33) into (31).

Similarly the thrust force is realized by solving the third scalar equation of (12) for T yields

$$T = \frac{m}{c_\theta c_\phi}(g - \ddot{z}_e). \tag{34}$$

Hence, the asymptotically stable virtual altitude dynamics of O_B is prescribed as follows

$$(\ddot{z}_e - \ddot{z}_{ed}) + c_5(\dot{z}_e - \dot{z}_{ed}) + c_6(z_e - z_{ed}) = 0 \tag{35}$$

where c_5 and c_6 are strictly positive scalars. The required control thrust T is obtained by solving (35) for $\ddot{z}_e$ and substituting in (34), resulting in

$$T = \frac{m}{c_\theta c_\phi}[g - \ddot{z}_{ed} + c_5(\dot{z}_e - \dot{z}_{ed}) + c_6(z_e - z_{ed})]. \tag{36}$$

5. INNER LOOP CONTROL DESIGN USING ARGDI

This section presents the ARGDI design of the three control torques required to track the reference roll, pitch and yaw attitude commands. We define the desired angular position and body rate vectors as

$$\boldsymbol{\Psi}_d = [\phi_r \ \theta_r \ \psi_d]^T, \qquad \boldsymbol{\Omega}_d = [p_d \ q_d \ r_d]^T \tag{37}$$

and define the state deviation function χ as

$$\chi = \mathbf{e}_o^T K \mathbf{e}_o \tag{38}$$

where $\mathbf{e}_o = \boldsymbol{\Psi} - \boldsymbol{\Psi}_d$, and K is a 3×3 positive-definite constant matrix. We now define the sliding mode variable s as

$$s = \dot{\chi} + a_1\chi + a_2 \int_0^t \chi dt \tag{39}$$

where a_1 and a_2 are positive constants. The time derivative of s given by (39) is evaluated as

$$\dot{s} = \ddot{\chi} + a_1\dot{\chi} + a_2\chi. \tag{40}$$

Hence, (asymptotic or finite-time) convergence of $\dot{s}$ to zero implies asymptotic convergence of χ, $\dot{\chi}$, and $\ddot{\chi}$ to zeros. Evaluating $\dot{\chi}$ and $\ddot{\chi}$ along solution trajectories of the Quadrotor's attitude dynamics given by (17) and (24) yields the following form of (40)

$$\dot{s} = \mathcal{A}\boldsymbol{\tau} - B \tag{41}$$

where

$$\mathcal{A} = 2\mathbf{e}_o^T K \mathbf{G} \tag{42}$$

and

$$B = -2\dot{\mathbf{e}}_o^T K \dot{\mathbf{e}}_o - 2a_1 \mathbf{e}_o^T K \dot{\mathbf{e}}_o - a_2 \mathbf{e}_o^T K \mathbf{e}_o - 2\mathbf{e}_o^T K(\mathbf{F} - \ddot{\boldsymbol{\Psi}}_d). \tag{43}$$

The expression of B given by (43) involves $\mathbf{F}$, which depends essentially on the Quadrotor's inertia parameters and angular speeds of the four rotors. Therefore, inaccuracies in attitude and attitude rate measurements adversely affect the computed online values of B. For that reason, we will assume that B is unknown and we will replace the function B in the proposed control law by an estimation variable $\hat{B}$ that will be updated adaptively as will be shown. The proposed ARGDI control law $\boldsymbol{\tau}$ is given by

$$\boldsymbol{\tau} = \overbrace{\mathcal{A}^*\hat{B} + \mathbf{P}\boldsymbol{\zeta}}^{\boldsymbol{\tau}_{eq}} - \overbrace{c\mathcal{A}^\star \text{sign(s)}}^{\boldsymbol{\tau}_{rbt}} \tag{44}$$

where $\boldsymbol{\tau}_{eq}$ is the GDI equivalent control part and $\boldsymbol{\tau}_{rbt}$ is the SMC robustifying control element. The dynamically scaled generalized inverse $A^\star$ is given by

$$\mathcal{A}^* = \frac{\mathcal{A}^T}{\mathcal{A}\mathcal{A}^T + \nu(t)} \tag{45}$$

where $\nu(t)$ satisfies the first-order forced dynamics

$$\dot{\nu}(t) = -\nu(t) + \gamma \frac{\|\mathbf{e}_i(t)\|^2}{\|\mathbf{e}_o(t)\|^2}, \ \gamma > 0, \ \nu(0) > 0 \tag{46}$$

where $\mathbf{e}_i = \boldsymbol{\Omega} - \boldsymbol{\Omega}_d$, and $\|\cdot\|$ denotes the Euclidean norm. In (44), $\mathbf{P}$ is the null projection matrix given by

$$\mathbf{P} = \mathbf{I}_{3\times 3} - \mathcal{A}^+\mathcal{A} \tag{47}$$

and $\boldsymbol{\zeta} \in \mathbb{R}^3$ is a null control vector that is designed to stabilize the Quadrotor's angular body rate dynamics. In this paper we utilize the design of $\boldsymbol{\zeta}$ that is given by Eq. (74) in Ansari et al. (2019b). The (discontinuous) SMC term $\boldsymbol{\tau}_{rbt}$ in the ARGDI control law given by (44) works to robustify the closed loop performance against modeling uncertainties and external disturbances and dynamic scaling of the MPGI, where c is a positive sliding mode constant gain, and sign(.) is the sign function. Substituting the expression of $\boldsymbol{\tau}$ given by (44) in (41) yields

$$\dot{s} = \delta_{\mathcal{A}}\hat{B} - c\delta_{\mathcal{A}}\text{sign(s)} - B \tag{48}$$

where $\delta_{\mathcal{A}} = \mathcal{A}\mathcal{A}^*$. Because $\nu \in (0, \infty)$, the expression of $\mathcal{A}^*$ given by (45) implies that $0 \leq \delta_{\mathcal{A}} < 1$. Let the unknown function B be the sum of the estimate $\hat{B}$ and an estimate error $\tilde{B}$. Then a stability condition of (48) is derived by considering the following Lyapunov function

$$V = \frac{1}{2}s^2 + \frac{1}{2\gamma_1}\hat{B}^2 + \frac{1}{2\gamma_2}\tilde{B}^2. \tag{49}$$

The time derivative of V is given by

$$\begin{aligned}
\dot{V} &= s\dot{s} + \frac{1}{\gamma_1}\hat{B}\dot{\hat{B}} + \frac{1}{\gamma_2}\tilde{B}\dot{\tilde{B}} \\
&= s\left(\delta_{\mathcal{A}}\hat{B} - c\delta_{\mathcal{A}}\text{sign(s)}\right) - s\hat{B} - s\tilde{B} \\
&\quad + \frac{1}{\gamma_1}\hat{B}\dot{\hat{B}} + \frac{1}{\gamma_2}\tilde{B}\dot{\tilde{B}} \\
&= s\delta_{\mathcal{A}}\hat{B} - s\hat{B} - c\delta_{\mathcal{A}}|s| - s\tilde{B} \\
&\quad + \frac{1}{\gamma_1}\hat{B}\dot{\hat{B}} + \frac{1}{\gamma_2}\tilde{B}\dot{\tilde{B}} \\
&= s(\delta_{\mathcal{A}} - 1)\hat{B} + \frac{1}{\gamma_1}\hat{B}\dot{\hat{B}} - c\delta_{\mathcal{A}}|s| \\
&\quad - \tilde{B}\left(s - \frac{1}{\gamma_2}\dot{\tilde{B}}\right) \\
&= \left(s(\delta_{\mathcal{A}} - 1) + \frac{1}{\gamma_1}\dot{\hat{B}}\right)\hat{B} - c\delta_{\mathcal{A}}|s| \\
&\quad - \tilde{B}\left(s - \frac{1}{\gamma_2}\dot{\tilde{B}}\right).
\end{aligned} \tag{50}$$

The expressions of $\dot{\hat{B}}$ and $\dot{\tilde{B}}$ are chosen as

$$\dot{\hat{B}} = -\gamma_1(k_1\hat{B} + s(\delta_{\mathcal{A}} - 1)) \tag{51}$$

$$\dot{\tilde{B}} = -\gamma_2(k_2\tilde{B} - s) \tag{52}$$

where $k_1, k_2 > 0$. Hence, $\dot{V}$ becomes

$$\dot{V} = -c\delta_{\mathcal{A}}|s| - k_1\hat{B}^2 - k_2\tilde{B}^2. \tag{53}$$

The obtained expression for $\dot{V}$ is only negative semi definite because $\delta_{\mathcal{A}}$ may take the zero value. Therefore, the conclusion that follows is that the points $s = 0$, $\hat{B} = 0$, and $\tilde{B} = 0$ are Lyapunov stable. Since V is non-increasing and

bounded from below, it must converge to a constant value. Moreover, Lyapunov stability of $s = 0$, $\hat{B} = 0$, and $\tilde{B} = 0$ implies boundedness of $\dot{s}$, $\dot{\hat{B}}$, and $\dot{\tilde{B}}$, which together with the boundedness of $\dot{\delta}_{\mathcal{A}}$ imply boundedness of the second derivative $\ddot{V}$. Therefore, $\dot{V}$ is uniformly continuous, and hence it follows from Barbalat's lemma that asymptotic convergence of V implies asymptotic convergence of $\dot{V}$ to zero. Therefore, $\hat{B}$, $\tilde{B}$ in addition to the product $\delta_{\mathcal{A}}|s|$ must converge to zero. Nevertheless, convergence of $\hat{B}$ and $\tilde{B}$ to zeros implies that the (unknown) function B converges to zero, which implies from (43) that $\mathbf{e}_o$ and $\dot{\mathbf{e}}_o$ must converge to zeros. Convergence of $\mathbf{e}_o$ to zero implies the convergence of $\mathcal{A}$ and $\delta_{\mathcal{A}}$ to zeros as inferred from (42), and the convergence of $\dot{s}$ to zero follows from (48).

The proposed ARGDI control law preserves the geometric structure of a conventional GDI control law. The ARGDI control law given by (44) can be rewritten as

$$\boldsymbol{\tau} = \underbrace{\mathcal{A}^*(\mathbf{x}_p, \nu, t)\{\hat{B} - c\,\mathrm{sign(s)}\}}_{\in \mathcal{R}(\mathcal{A}^T)} + \underbrace{\mathbf{P}(\mathbf{x}_p, t)\boldsymbol{\zeta}}_{\in \mathcal{N}(\mathcal{A})} \tag{54}$$

which consists of two parts that act on two orthogonally complement subspaces of the control space: a particular part that acts on the range space $\mathcal{R}(\mathcal{A}^T)$ and an auxiliary part that acts on the nullspace $\mathcal{N}(\mathcal{A})$. This mutual orthogonality of the two control subspaces allows to design the particular control law independently from the auxiliary control law.

6. SIMULATIONS AND EXPERIMENTAL VALIDATION

To illustrate the performance of the proposed two-loops control methodology, numerical simulation was created in Matlab/Simulink environment. Computer simulation is performed on a six DOFs quadrotor simulator whose nominal inertia and aerodynamic parameters are listed in Table 1. Moreover, lab experiments are also conducted to

Table 1. Quanser's 3 DoF Hover specifications

Parameters	Description	Value	Unit
m	mass	2.850	kg
d	arm length	0.280	m
I_x	inertia	0.055	$kg.m^2$
I_y	inertia	0.055	$kg.m^2$
I_z	inertia	0.110	$kg.m^2$
b	thrust factor	$0.877e^{-5}$	–
k	drag factor	$1.527e^{-4}$	–

visualize real time closed loop performance on Quansers 3 DOF Hover test bed.

6.1 Computer Simulation

In computer simulations, the capability of proposed two-loop controller is tested using Matlab/Simulink software. The helical trajectory with variable amplitude is commanded For pitch and roll axis, the tracking of desired sinusoidal profiles is validated, where the commanded sinusoidal positional coordinates are governed by the following kinematical equations

$x_{ed}(t) = \pm A_m \sin(2\pi f t), \;\; y_{ed}(t) = \pm A_m(t) \sin(2\pi f t + \pi/2)$

where maximum value of A_m is 10 m. The desired altitude profile is defined as $z_{ed}(t) = t$. A realistic scenario is demonstrated by introducing 20% random variations in the aerodynamic coefficients and inertial parameters, to gain a qualitative insight of the robustness characteristic and sensitivity of proposed two-loop control architecture. In simulation nominal parameters are considered to model the plant however these parameters are assumed to be unknown for ARGDI and are estimated online in the sense of Lyapunov. The key performance indices such as

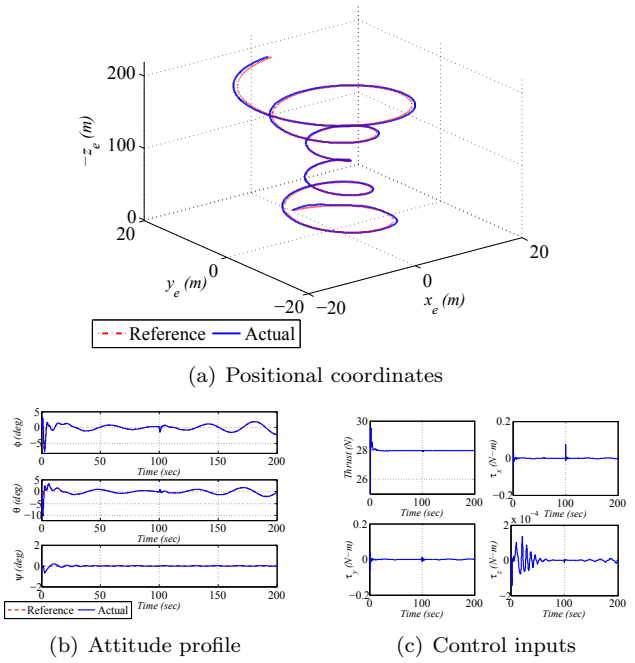

(a) Positional coordinates

(b) Attitude profile

(c) Control inputs

Fig. 1. Helical trajectory

positional coordinates, attitude tracking curves, and the control inputs are shown in Figs. 1(a)-1(c). The positional response curve in three dimensions is shown in Fig. 1(a) which demonstrate effective tracking of the helical path. The ARGDI control realizes better attitude tracking curves with fast convergence as shown in Fig. 1(b). The corresponding thrust input and control torques are shown in Fig. 1(c) which reveals none of them achieved the saturation limit. Hence the proposed methodology is robust against parametric variations and proven to be effective for wider range of operations.

6.2 Experimental Results

To further verify and examine the stabilization and tracking response of ARGDI based attitude control, an experiment is performed on Quansers 3DOF Hover test bed. The hover system consists of a frame with four propellers and is mounted on an air bearing joint such that it rotates freely in all the three rotational axes. Encoders are used to measure the angular positions for yaw, pitch and roll channels. In the experiment the sinusoidal inputs are commanded to the pitch and roll axis which are defined as

$$\theta_d(t) = \pm 5 \sin(2\pi f t), \qquad \phi_d(t) = \pm 5 \sin(2\pi f t + \pi/2)$$

whereas the desired yaw angle is set to be zero. The experimental curves using ARGDI control are summarized in Figs. 2(a)- 2(b). The time histories of attitude tracking curves are shown in Fig. 2(a) which demonstrate better

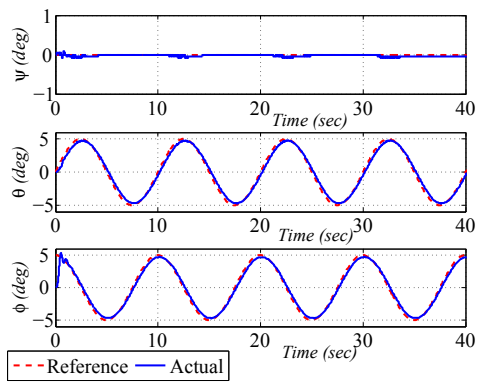

(a) Attitude profile

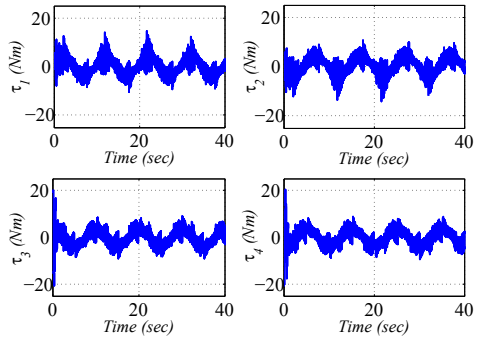

(b) Control torques

Fig. 2. Experimental results

and accurate tracking performance. Moreover corresponding control torques are shown in Fig. 2(b) depict that the commanded torques are remain within the reasonable range and never saturate. The experimental studies demonstrate the tracking capability of ARGDI control in the presence of significant inherent uncertainties in the physical parameters of the hover test bed and proves to be competent enough for its real time application to the complex nonlinear systems.

7. CONCLUSION

In this paper, a six DOF model of quadrotor vehicle is implemented with the intention to evaluate the performance of a continuous two loops control architecture for stabilization and tracking problem of this complex, open-loop unstable flying vehicle. In the outer loop, PD controller generates the desired tilting commands along with required thrust to control quadrotor position in three dimensional inertial space. The inner loop exploit the attributes of ARGDI control to guarantee finite time attitude tracking along with online estimation of systems unknown dynamical parameters. Lyapunov stability principle is employed to establish the finite time stability of the closed loop system. Numerical simulation and real time experiments are presented to evaluate the performance of the developed control system.

REFERENCES

Ansari, U. and Bajodah, A.H. (2017a). Robust generalized dynamic inversion based control of autonomous underwater vehicles. *Proceedings of the Institution of Mechanical Engineers, Part M: Journal of Engineering for the Maritime Environment*, 232(4), 434–447.

Ansari, U. and Bajodah, A.H. (2017b). Robust launch vehicles generalized dynamic inversion attitude control. *Aircraft Engineering and Aerospace Technology*, 89(6), 902–910.

Ansari, U., Bajodah, A.H., and Hamayun, M.T. (2019a). Quadrotor control via robust generalized dynamic inversion and adaptive non-singular terminal sliding mode. *Asian Journal of Control*. doi:10.1002/asjc.1800.

Ansari, U., Bajodah, A.H., and Kada, B. (2019b). Development and experimental investigation of a quadrotors robust generalized dynamic inversion control system. *Nonlinear Dynamics*, 96(2), 1541–1557.

Ansari, U., Mehedi, I.M., Bajodah, A.H., and Al Saggaf, U.M. (2018). Positional control of rotary servo cart system using generalized dynamic inversion. *Journal of Vibroengineering*, 20(6), 2403–2413.

Bouabdallah, S., Noth, A., and Siegwart, R. (2004). Pid vs lq control techniques applied to an indoor micro quadrotor. In *Intelligent Robots and Systems, 2004.(IROS 2004). Proceedings. 2004 IEEE/RSJ International Conference on*, volume 3, 2451–2456. IEEE.

Das, H. (2018). Dynamic inversion control of quadrotor with a suspended load. *IFAC-PapersOnLine*, 51(1), 172–177.

Falanga, D., Foehn, P., Lu, P., and Scaramuzza, D. (2018). Pampc: Perception-aware model predictive control for quadrotors. In *2018 IEEE/RSJ International Conference on Intelligent Robots and Systems (IROS)*, 1–8. IEEE.

Kasdin, N.J. and Paley, D.A. (2011). *Engineering Dynamics*. Princeton University Press.

L'afflitto, A., Anderson, R.B., and Mohammadi, K. (2018). An introduction to nonlinear robust control for unmanned quadrotor aircraft: How to design control algorithms for quadrotors using sliding mode control and adaptive control techniques [focus on education]. *IEEE Control Systems*, 38(3), 102–121.

Leishman, J. (2002). *Principles of Helicopter Aerodynamics*. Cambridge University Press.

Mahony, R., Kumar, V., and Corke, P. (2012). Multirotor aerial vehicles: Modeling, estimation, and control of quadrotor. roboticsautomationmagazine, 19, 20-32. *Mayhew et al. C. Mayhew, R. Sanfelice, and A. Teel. On path-lifting mechanisms and unwinding in quaternion-based attitude control. Automatic Control, IEEE Transactions on. PP (99)*, 1–1.

Nelson, R. (1997). *Flight Stability and Automatic Control*. McGraw-Hill, New York, second edition.

Poultney, A., Gong, P., and Ashrafiuon, H. (2019). Integral backstepping control for trajectory and yaw motion tracking of quadrotors. *Robotica*, 37(2), 300–320.

Vitzilaios, N.I. and Tsourveloudis, N.C. (2009). An experimental test bed for small unmanned helicopters. *Journal of Intelligent and Robotic Systems*, 54(5), 769–794.

Zhou, F., Zhou, Y.J., Jiang, G.P., and Cao, N. (2018). Adaptive tracking control of quadrotor uav system with input constraints. In *2018 Chinese Control And Decision Conference (CCDC)*, 5774–5779. IEEE.